ELSEVIER

Journal of Hazardous Materials A121 (2005) 23–30

Journal of Hazardous Materials

www.elsevier.com/locate/jhazmat

Experimentally validated 3-D simulation of shock waves generated by dense explosives in confined complex geometries

Fotis Rigas *, Spyros Sklavounos

National Technical University of Athens, School of Chemical Engineering, 15700 Athens, Greece

Received 27 April 2004; received in revised form 18 January 2005; accepted 20 January 2005

Abstract

Accidental blast wave generation and propagation in the surroundings poses severe threats for people and property. The prediction of overpressure maxima and its change with time at specified distances can lead to useful conclusions in quantitative risk analysis applications. In this paper, the use of a computational fluid dynamics (CFD) code CFX-5.6 on dense explosive detonation events is described. The work deals with the three-dimensional simulation of overpressure wave propagation generated by the detonation of a dense explosive within a small-scale branched tunnel. It also aids at validating the code against published experimental data as well as to study the way that the resulting shock wave propagates in a confined space configuration. Predicted overpressure histories were plotted and compared versus experimental measurements showing a reasonably good agreement. Overpressure maxima and corresponding times were found close to the measured ones confirming that CFDs may constitute a useful tool in explosion hazard assessment procedures. Moreover, it was found that blast wave propagates preserving supersonic speed along the tunnel accompanied by high overpressure levels, and indicating that space confinement favors the formation and maintenance of a shock rather than a weak pressure wave.

Keywords: Shock wave; Detonation; Overpressure; Explosives; CFD; Explosion simulation

1. Introduction

The study of the generation and propagation of blast waves were always of great importance from the safety viewpoint for any chemical industry handling explosive materials or flammable gases. A large number of past explosion accidents has led to considerable property damages, in addition to human injuries along with fatalities in some cases [1].

In fact, risk analysis procedures applied in dangerous installations focus on the quantitative consequence estimation of potential accidental events (explosion, fire, toxic dispersion) aiming at the determination of hazardous zones in the vicinity. With regard to the explosives industries, where the main hazard arises from potential explosions, the interest concerns the evaluation of the effects of the shock wave generated by such energetic events. Usually, the criterion for a certain level of damage is the maximal (peak) overpressure predicted to developing at specified distances of interest [2–4].

The major characteristic for any explosion is the rapid release of a huge amount of energy in time intervals of the order of microseconds, which results in sharp local pressure increase. Subsequently, an overpressure wave is generated that propagates in three dimensions with velocity that exceeds the velocity of sound (supersonic flow) covering soon large distances. Possible explosion sources may be condensed phase materials, or flammable gas–air mixtures in confined (or not) space (confined and unconfined vapor cloud explosion, respectively). Condensed phase sources are meant highly exothermic chemical substances that are designed to explode, namely to release their energy quite rapidly, and they include high (or dense) explosives, solid propellants, and mixtures of fuels and oxidizers [5].

Among the widely employed semi-empirical methods for blast overpressure estimation (TNT equivalence, Baker–Strehlow, TNO multi-energy), the TNT equivalence is the only one that can be recommended for high explo-

* Corresponding author. Tel.: +30 2107723267; fax: +30 2107723163.
E-mail address: rigasf@central.ntua.gr (F. Rigas).

0304-3894/$ – see front matter © 2005 Elsevier B.V. All rights reserved.
doi:10.1016/j.jhazmat.2005.01.031

Nomenclature

d_p	density of the explosive material (kg m^{-3})
E_r	explosion power (kg m^2 s^{-3})
k	turbulence kinetic energy per unit mass (m^2 s^{-2})
M_p	explosive mass (kg)
r^n	residuals in the linearized system of equations
R_p	radius of the spherical explosive mass (m)
S	step function expressing the energy production within the domain during the explosion phase (kg m^2 s^{-3})
t	time (s)
t_0	time of explosion initiation (s)
t_1	energy release duration (s)
t_c	time constant equal to 1 s
U	detonation velocity (m s^{-1})
V	volume of integrated cell (m^3)
V_p	volume of the explosive sphere (m^3)
X, Y	horizontal coordinates (m)
Z	vertical coordinate (m)

Greek letters

α_1	dimensionless constant
ΔH_p	mass specific energy (J kg^{-1})
μ_t	turbulence dynamic viscosity (kg m^{-1} s^{-1})
ν_t	turbulence kinematic viscosity (m^2 s^{-1})
ρ	density (kg m^{-3})
φ	general scalar variable
φ^0	solution field in the first order Backward Euler scheme
φ^{00}	solution field in the second order Backward Euler scheme
ω	turbulent frequency (s^{-1})

Subscripts

i	the identifying number of the finite volume or node

sives [6]. However, the assumption of an equivalent mass of TNT does not allow for the characteristics of the explosion, whilst the way it affects the surroundings is independent of the explosion source. In fact, material physical properties play important role in blast wave characteristics; for example, higher explosive density entails higher detonation velocity and hence greater rate of energy release resulting in enhanced overpressure levels [7].

Alternatively, numerical techniques may be applied to describe detonation events. Computational approximations of explosions have been performed in previous papers using two-dimensional, time-dependent conservation equations [8,9]. This work aims at testing the suitability of the three-dimensional CFD code CFX 5.6 on the simulation of shock wave propagation in a confined complex geometry. Some discussion for the computational capabilities of the code has been made in a previous paper [10]. The simulation presented in this paper deals with the experimental work of Binggeli et al. [11], in which dense explosive detonation test took place in a small-scale branched closed tunnel. This latter experimental work performed to study the propagation of the shock wave in a complicated tunnel by logging overpressure histories prior to branching, as well as at certain points in the branches. The explosive used in the experiment was Plastit, a solid energetic material used mainly for military purposes. Like most dense explosives, it has the property of exploding at essentially constant rate, namely with constant detonation velocity [12].

In the simulation procedure, the detonation duration and energy release rate were defined for the current explosive material (Plastit) using its physical properties (mass specific energy, density, detonation velocity), by a properly adapted step function for the energy production term. Proceeding on the discretisation of the domain, besides selective mesh refinement of the initial unstructured tetrahedral mesh (techniques that have been also used in other explosion codes [13,14]), there was the possibility for inflation layers construction on the walls of the domain, allowing for better modeling of the close-to-wall physics where large variations of fluid properties occur.

The obtained overpressure maxima and wave structures were compared against the corresponding experimental ones with a fairly good agreement, showing that CFDs are able to predict potential explosion effects in complex confined space configurations. Moreover, velocity visualizations within the domain revealed that blast wave propagates preserving supersonic speed along the narrow part of the arrangement developing at the same time high overpressures. In contrast, within the free-field part, wave speed turns abruptly to subsonic accompanied by significant overpressure drop. This indicates an important role of space confinement during an explosion, since it favors the formation of a shock rather than a weak pressure wave, thus increasing the risk for destructive effects.

2. Numerical methods

2.1. Governing equations

The CFX code has been designed to solve transonic and supersonic flows, even for Mach numbers bigger than 2, yet with slow convergence rates, as observed during the simulations. The set of equations considered in the code for the conservation of mass, momentum and energy are the unsteady Navier–Stokes equations in their conservation form [15,16].

In supersonic flows or when sharp shocks appear in the domain, the kinetic energy effects cannot be neglected any more as happens in low speed flows. Total energy model incorporated in CFX code predicts the temperature in the entire domain accounting for heat transfer by conduction, convection, turbulent mixing and viscous work. This model is essential for Mach numbers up to 2 and besides kinetic

energy effects, it takes into account buoyancy effects arisen by hot spots in the domain (i.e. due to thermal sources) and hence large local density variations.

2.2. Turbulence modeling

A number of models have been developed that can be used to approximate turbulence based on the Reynolds Averaged Navier–Stokes equations and can be classified as either eddy viscosity or Reynolds stress models [16].

The SST model [17,18] used in the computations was designed to give highly accurate predictions of the onset and the amount of flow separation under adverse pressure gradients by the inclusion of transport effects into the formulation of the eddy-viscosity, resulting in major improvement of flow separation prediction capability. The proper transport behavior is obtained by a limiter to the formulation of the eddy-viscosity:

$$v_t = \frac{\alpha_1 k}{[\max(\alpha_1 \omega, SF)]} \tag{2.1}$$

where

$$v_t = \frac{\mu_t}{\rho} \tag{2.2}$$

F is a blending function of the distance to the nearest wall and the flow variables k, ω, which restricts the limiter to the wall boundary layer, while S is an invariant measure of the strain rate.

2.3. Grid generation

The numerical method used for the discretisation of the computational domain was the finite volume method (FVM) [19], which has been utilized in explosion studies for 2-D discretisation with unstructured triangular grid [14]. This approach involves the subdivision of the entire domain into finite control volumes (cells) using a grid (mesh). The governing equations are integrated over each control volume, such that the relevant quantity (mass, momentum, energy, etc.) is conserved in a discrete sense for each cell.

The current version of CFX code incorporates the ANSYS ICEM CFD 4 meshing tool. The full construction of the mesh is performed in two steps: Initially, the domain volume is filled with tetrahedral cells, whilst a triangular surface mesh is generating on the overall object surface. For improving cells quality, a power smoothing algorithm as well as a variety of tools for local mesh adaptation and refinement is available. Mesh construction parameters (such as scale factor and maximum element size) are user defined. Thus, particular care should be given in order to an optimal mesh be built: neither too coarse (because then the solution may not be satisfactorily accurate and significant deviations from the real values may arise), nor too refined (since extremely refined meshes may demand excess CPU time to execute a simulation). The latter depends strongly upon the computational power available.

In the second step, the generation of hybrid tetrahedral grids (the so-called inflation layers) consisting of layers of triangular prism elements on the boundary surfaces and tetrahedral elements in the interior is carried out. In contrast with pure tetrahedral meshes, hybrid tetrahedral meshes with near-surface prism layers allow for better modeling of the close-to-wall physics of the flow field (i.e. sharp velocity changes) giving rise to more accurate results.

2.4. Solution scheme

Analytical solutions to the Navier–Stokes equations exist for only the simplest of flows under ideal conditions [20]. To obtain solutions for real flows, a numerical approach must be adopted whereby the equations are replaced by algebraic approximations which can be solved using a numerical method.

The solution to the conservation equations via FVM proceeds through the integration of the governing partial differential equations over all the control volumes (3-D elements). Afterwards, the integral equations obtained are converted to a system of algebraic equations. The latter are solved iteratively at nodal points inside each cell aiming at minimization of the residuals (iteration loop error) until the desired convergence be satisfied.

CFX 5.6 uses a coupled solver, which solves the hydrodynamic equations (for pressure and velocity components) as a single system. This solution approach uses a fully implicit discretisation of the equations at any given time step reducing the number of iterations required for convergence. The general solution algorithm is illustrated in Fig. 1.

In this work, in order to obtain a solution to the transient problem, the second order Backward Euler transient scheme was employed, which is applicable for constant and variable step sizes. The second order Backward Euler method is an implicit time-stepping scheme and, in contrast with that of

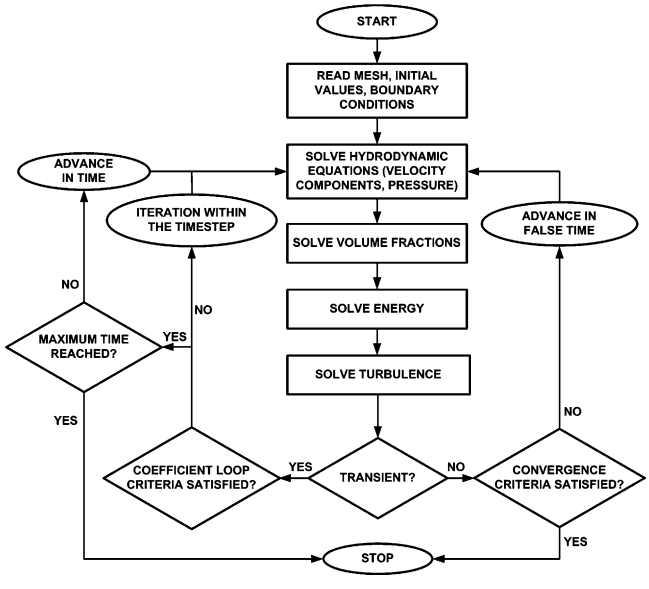

Fig. 1. Solving algorithm in CFX 5.6.

first order, is second order accurate in time. However, it is not monotonic and therefore inappropriate for some quantities that must remain bounded, such as turbulence quantities. Consequently, the first order Backward Euler scheme was applied as far as turbulence equations are regarded.

The first order Backward Euler scheme approximates the transient term as:

$$\frac{\partial(\int_v \rho\varphi \, \mathrm{d}v)}{\partial t} = \frac{\rho V(\varphi - \varphi^0)}{\Delta t} \tag{2.3}$$

It is robust, fully implicit, bounded, conservative in time, and does not create a time step limitation. The transient term has no bearing on the steady state solution, but it is only first order accurate in time and therefore may induce numerical diffusion in time.

The second order Backward Euler scheme approximates the transient term as:

$$\frac{\partial(\int_v \rho\varphi \, \mathrm{d}v)}{\partial t} = \frac{\rho V}{\Delta t(1.5\varphi - 2\varphi^0 + 0.5\varphi^{00})} \tag{2.4}$$

where φ^{00} represents the solution field from the time step before the old time level. This scheme is also robust, implicit, conservative in time, and does not create a time step limitation [20].

Solution fields are stored at the mesh nodes. Nevertheless, various terms in the equations require solutions or solution gradients to be evaluated at integration points, so there must be a way to calculate the solution variation within an element. This is achieved by means of finite element shape functions [16], according to which a variable φ varies within an element as follows:

$$\varphi = \sum_{i=1}^{N_{\mathrm{mode}}} (N_i \varphi_i) \tag{2.5}$$

where N_i is the shape function for i-node, φ_i the value of φ at the same nodal point and the summation is referred to the over all nodes of the volume element.

The numerical technique utilized for the completion of the advection term discretisation was the first order upwind differencing scheme (UDS) [19]. Difference schemes in their majority are based on series expansion approximations (such as the Taylor series) for continuous functions. UDS is very robust, namely numerically stable, and is guaranteed to not introduce non-physical overshoots or undershoots in the solution.

At the last step, the linear set of equations that arise by applying the FVM to all elements in the domain are discrete conservation equations. The system of equations can be written in the form:

$$\sum_{nb_i} a_i^{\mathrm{nb}} \phi_i = b_i \tag{2.6}$$

where φ is the solution, b the right-hand side, a the coefficients of the equation, i the identifying number of the finite volume or node in question, and nb means "neighbour", but also includes the central coefficient multiplying the solution at the ith location. The node may have any number of such neighbours, so that the method is equally applicable to both structured and unstructured meshes. The set of these, for all finite volumes constitutes the whole linear equation system and can be written in the general matrix form:

$$[A][\varphi] = [b] \tag{2.7}$$

where $[A]$ is the coefficient matrix, $[\varphi]$ the solution vector and $[b]$ the right-hand side.

The above equation can be solved iteratively by starting with an approximate solution, φ^n, that is to be improved by a correction, φ', to yield a better solution, φ^{n+1}, i.e.

$$\varphi^{n+1} = \varphi^n + \varphi' \tag{2.8}$$

where φ' is a solution of

$$\dot{A}\varphi' = r^n \tag{2.9}$$

with r^n, the residual, obtained from

$$r^n = b - A\varphi^n \tag{2.10}$$

Repeated application of this algorithm will normally yield a solution of the desired accuracy.

3. Simulation set up

3.1. Experimental set up

The experiment belongs to an experimental research program of NC Laboratory Spiez for investigating the effects of detonations and resulting blast wave propagation in closed tunnel systems. The experiment implementation dealt with a high explosive (Plastit) detonation in the arrangement shown in Fig. 2. The purpose was to study the propagation of the shock wave in the complicated tunnel by obtaining overpres-

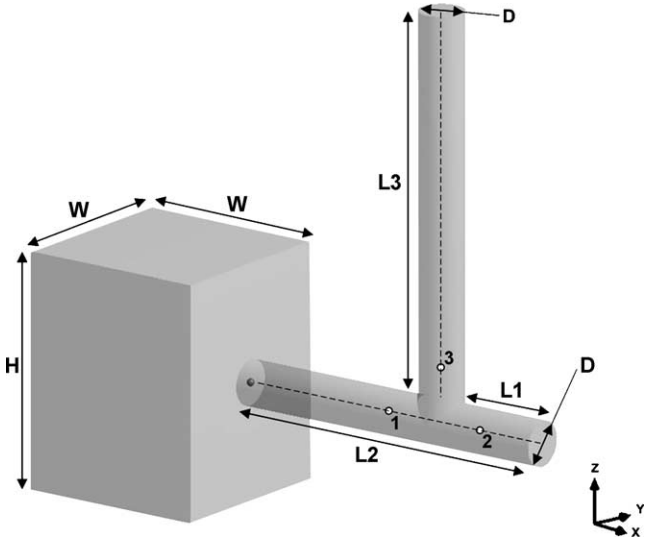

Fig. 2. Experimental configuration built in CFX code.

Table 1
Plastit properties and calculated parameters entered into the step function (Eq. (3.1))

Step function terms	Properties			Calculated parameters	
Physical quantities	Mass specific energy (kJ/kg)	Density (kg/m^3)	Detonation velocity (m/s)	Detonation duration (s)	Energy release rate (kg m^2 s^{-3})
Input values	4870	1580	8500	165.8 × 1E−8	54351 × 1E6

sure histories measurements prior to the bifurcation, as well as at certain points in the branches of the tunnel.

The experimental set up consisted of a branched cylindrical section connected in one side with a box of relatively large dimensions. The blast charge had spherical shape and mass equal to 0.0185 kg (500 kg in full scale), while it was situated in the middle of the cross-section between the tunnel and the box's free field. The cross section of 1:30 scaled tunnel was circular with a diameter of 0.168 m corresponding to 5 m in full scale.

The airblast propagation was studied in the L-shaped tunnel and transient overpressure levels were measured at points 1 (before the branch), 2 and 3 (after the branch). All measurement points (MP) were laid on the axis of symmetry of each tunnel. The dimensions presented in Fig. 1 are equal to: H: 0.868 m, W: 0.7 m, D: 0.168 m, L_1: 0.360 m, L_2: 1.280 m and L_3: 1.416 m. The distances of MP1 and MP2 from the center of blast charge were 0.668 and 1.004 m, respectively, whereas the distance between MP3 and the horizontal axis of symmetry was equal to D.

3.2. Input data definition

The adiabatic (no heat transfer) wall boundary condition was imposed for the sides of the pipes and the cube. As discussed above, condensed explosives have the property of exploding at constant rate (detonation velocity), whose value hangs on material density and type. For that reason, it would be a good approximation, if the source term were given through a properly adapted step function (S) expressing the energy production within the domain:

$$S = E_r \times \text{step}\left(\frac{-(t-t_0)(t-t_1)}{t_c^2}\right) \quad (3.1)$$

where t represents the time (s), $t_0 = 0$ s, $t_c = 1$ s, t_1 = detonation duration (s) and E_r the energy release rate or explosion power (kg m^2 s^{-3}).

The unknown terms on the right-hand side may be found (or indirectly calculated) by experimental data available in the literature in relation with the explosive material employed [12]. In Table 1, Plastit properties and calculated parameters relative to Eq. (3.1) are tabulated. The detonation duration (t_1) is calculated by dividing the detonation velocity (U) with the radius of the spherical explosive mass (R_p): $t_1 = U/R_p$. The radius is calculated as a function of the volume of the sphere (V_p), which is found by dividing the explosive mass (M_p) with the density (d_p): $V_p = M_p/d_p$. The last term E_r (J s^{-1}) is given from the relation: $E_r = (\Delta H_p \times M_p)/t_1$, where ΔH_p is the mass specific energy (J kg^{-1}).

4. Computational results and discussion

4.1. Validation

The mesh on the 3-D computational domain was constructed after deciding for a refinement of the volume elements bounded on tunnel sides, in addition to the creation of inflation layers on the box and tunnel walls. Adaptive grid techniques have been also incorporated in other explosion codes for the refinement of domain regions of major interest [13]. The ultimate grid consisted of 33,450 volume elements, from which 24,620 were tetrahedrons and 8830 were prisms. In Fig. 3 the inflation layers on the tunnel walls as well as the refined section of the mesh are presented.

The solution of the problem was divided into two stages. First, an initial values file was obtained by solving the problem in steady state. Then, the transient solution proceeded for total simulation time equal to 0.01 s by giving very small time steps varied from 1E−9 to 1E−5 s as follows: 10 × 1E−9 + 9 × 1E−8 + 9 × 1E−7 + 9 × 1E−6 + 999 × 1E−5. The convergence criterion for the transient run was the residual RMS (residual of root mean square) to be equal to or less than 1E−4, but for the steady state was set one order of magnitude lower (1E−5). The latter led to relatively large number of iterations (415) until the desired accuracy was achieved. Regarding the transient runs, the number of iterations was fluctuating between four and six per time step. The transient

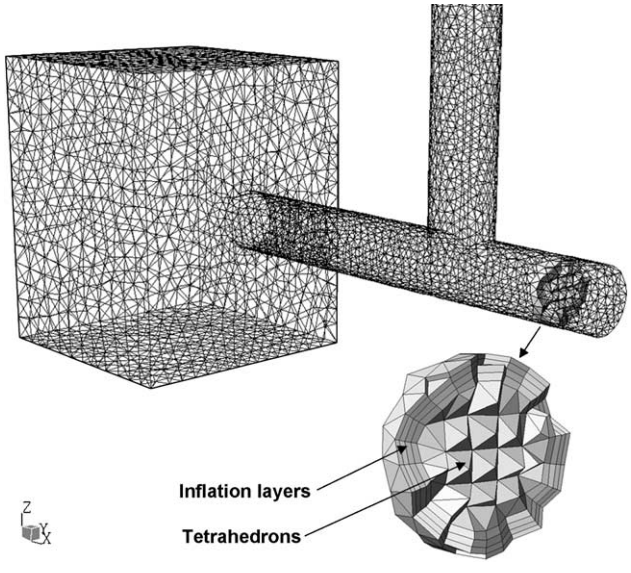

Fig. 3. Computational grid and selective mesh refinement in the tunnel segment. Tetrahedral elements and inflation layers are also illustrated on a transversal cross section of the tunnel.

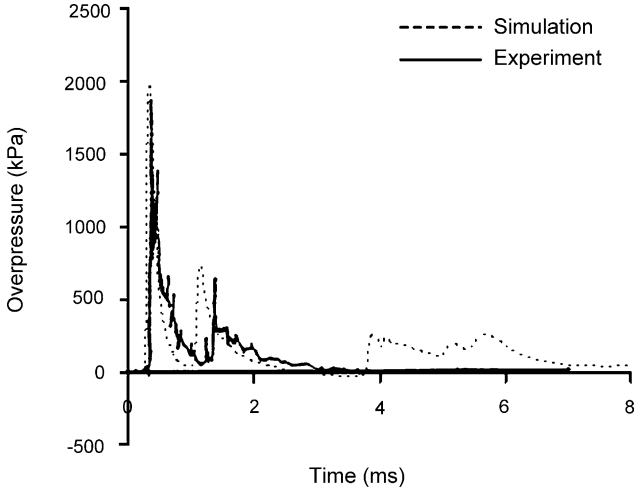

Fig. 4. Predicted and experimental overpressure–time plots at point 1.

simulation required approximately 50 h clock time (CPU time $1.5 \times 1E5$ s) for full execution on an 800 MHz Intel® Celeron processor with 512 MB RAM.

Computational relative pressure curves are plotted versus time in Figs. 4–6 for the measurement points 1, 2 and 3, respectively. The corresponding experimental curves are also shown in the same plots. Simulation results are obviously in reasonably good agreement with the experimental records. The difference between computational and experimental overpressure curves lies in overestimation of overpressure maxima (peak overpressures), yet without noticeable temporal divergence. The relative errors for computed peak overpressures fall into the range between 8 and 18% (Table 2) confirming a reasonably good approximation of the experimental maxima. The relative errors for arrival times (namely the time that pressure starts rising up) and impulse (pressure × duration) are displayed in Tables 3 and 4, respectively. It is evident that the code predicts successfully the explosion front passage through all measurement points, as well as the impulse of the blast wave on them.

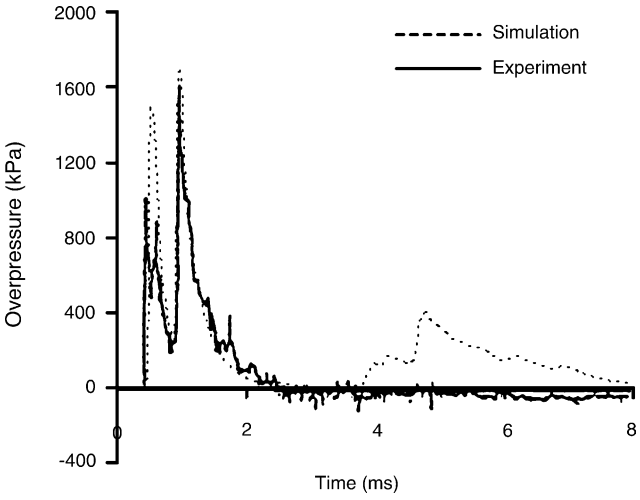

Fig. 5. Predicted and experimental overpressure–time plots at point 2.

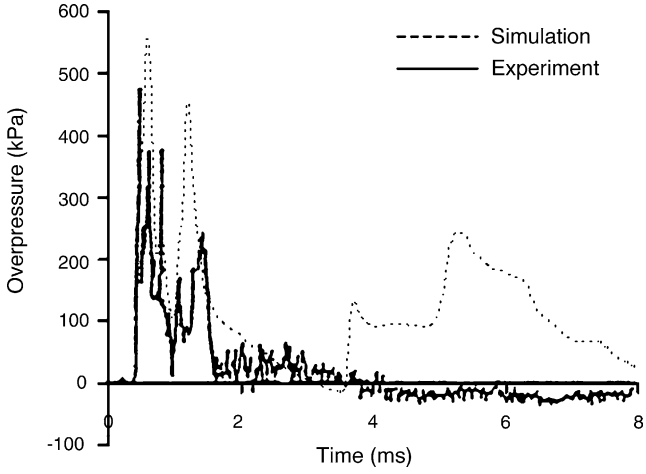

Fig. 6. Predicted and experimental overpressure–time plots at point 3.

Table 2
Relative errors between computational and experimental peak overpressures

Measurement points	Experimental value (kPa)	Computational value (kPa)	Relative error (%)
Point 1	1850	2009	+8.6
Point 2	1600	1720	+7.5
Point 3	465	550	+18.2

Table 3
Relative errors between computational and experimental arrival times

Measurement points	Experimental value (ms)	Computational value (ms)	Relative error (%)
Point 1	0.30	0.250	−16.7
Point 2	0.44	0.46	+4.5
Point 3	0.43	0.39	−9.3

One reason for the deviations appearing in Figs. 4–6 is the simplifying assumptions on problem physics definitions; in particular, the air in the tunnel was considered as an ideal instead of real gas. This was necessary in order to take into account in the computations the high compressibility effects within the flow field of the current problem. However, the behavior of air as a real gas differs significantly from that of the ideal one when the pressure takes extremely high values due to explosion front passage. With regard to peak overestimation, a possible explanation could be the heat loss that actually happens through the pipe sides, and which was not taken into account in the simulation. The latter means that an additional temperature increase is calculated leading according to the gas law to additional pressure increase. Furthermore, a much more refined mesh could probably yield a more precise solu-

Table 4
Relative errors between computational and experimental impulses

Measurement points	Experimental value (kPa s)	Computational value (kPa s)	Relative error (%)
Point 1	1335	1273	+4.9
Point 2	1726	1553	+11.1
Point 3	721	558	+29.2

tion, leading however to significant enhancement of the computational time. On the other hand, this overestimation might be considered tolerable from the safety point of view, since it would lead to overestimation of the explosion hazard in accident scenarios and hence to conservative risk assessment. The pressure increase appearing after about 4 ms in the numerical calculations was not observed in the experiments. This differentiation could result from the reflections of the explosion front at the end of the tunnel and the concurrent heat losses, which have not been included in the computational procedure.

It is worthwhile mentioning that a simulation of the current experiment via the two-dimensional explosion code AUTODYN-2D was performed in the work of Binggeli et al. [11], providing results comparable to those computed in this paper.

4.2. Pressure and velocity profiles

In Figs. 7 and 8, pressure and velocity profiles have been plotted inside the computational domain before and after the passage of the shock wave from the bifurcation at times 0.25 and 0.60 ms, respectively. As someone can see in Figs. 7a and 8a, the confinement of the right-hand space (tunnel field) does not allow the free expansion of high kinetic energy gas molecules, as in the left-hand space (box free field), thus leading to enhanced pressures in the right-hand side.

Likewise, the propagation velocity of the shock wave in the left-hand side (free-field of the domain) reduces rapidly taking values lower than the speed of sound (subsonic flow). On the contrary, the shock wave propagating in the tunnel field preserves speed higher than that of sound rendering the flow supersonic (Figs. 7b and 8b). Consequently, it may be concluded that long narrow geometries contribute to increase of the blast wave front velocity and pressure. This indicates an important role of space confinement during an explosion, since it favors the formation of a shock rather than a weak pressure wave aggravating the impact on humans and structures.

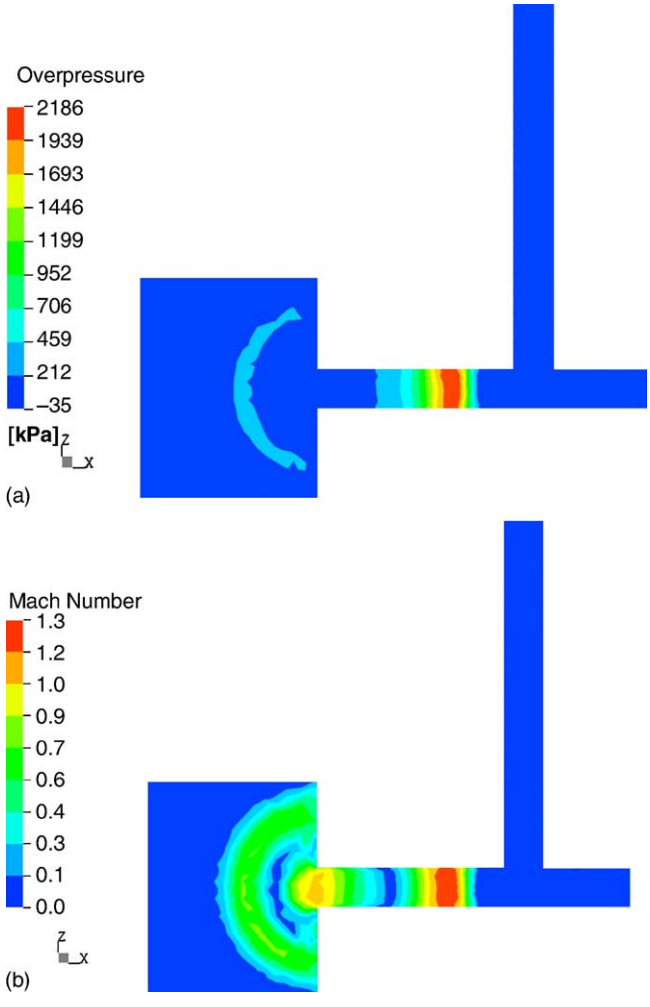

Fig. 7. Snapshot of overpressure (a) and Mach number (b) profiles within the computational domain in an early stage of shock wave propagation (time = 0.25 ms).

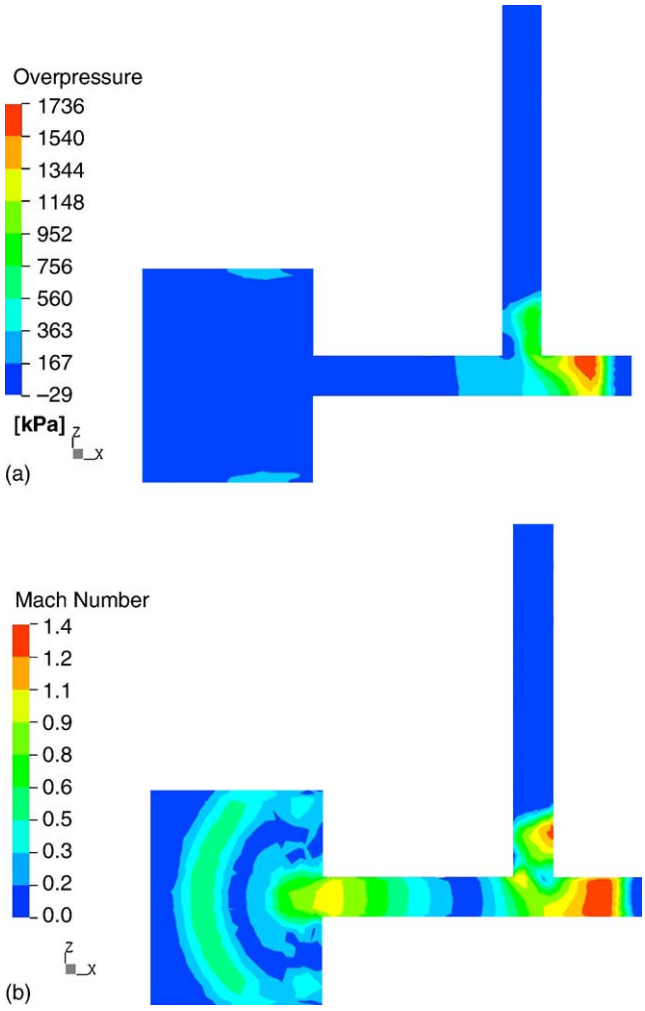

Fig. 8. Snapshot of overpressure (a) and Mach number (b) profiles within the computational domain after the bifurcation (time = 0.60 ms).

Comparing the peak overpressures tabulated in Table 2, it is apparent that overpressure maxima developed in the branched tunnel are substantially smaller than that in the straight tunnel. This may be of vital importance for the explosive industry as a safety measure for application in potential explosion accidents in confined spaces where explosive materials are treated, or even for emergency corridors construction in subway tunnels whose configuration is similar to the studied one.

5. Conclusions

In this paper, a 3-D simulation of the shock wave propagation produced by a dense explosive detonation in a small-scale complex tunnel configuration was attempted. The main purpose was to obtain and validate predictions of overpressure histories, as well as to study the way that the resulting shock wave propagates within the confined space applying computational fluid dynamics techniques.

The comparison of numerical results with experimental measurements showed noticeable good agreement, especially with regard to arrival time predictions of the explosion front. Computed overpressure maxima were generally overestimated in relation with the experimental ones, however with reasonable relative errors.

The study of velocity profile within the domain showed that the shock wave preserves supersonic propagation speed inside the narrow tunnel space (Mach number $\cong 1.3$) for a relatively long distance. At the same time, propagation speed decreases sharply in the free-field becoming subsonic (Mach number $\cong 0.7$) after a short distance. This indicates the important role of space confinement during an explosion, since it favors the formation of a shock rather than a weak pressure wave, which aggravates the effects of the blast on the surroundings.

In summary, the proximity between numerical predictions and experimental results confirms that CFDs can be effectively used in explosion hazard estimation procedures even in confined spaces of complex geometry, where sudden and complicated flow phenomena arise.

Acknowledgements

This work was supported by the Ministry of National Education and Religious Affairs (Community Support Framework 2000–2006) under the HERACLITUS research program.

References

[1] Z. Guoshun, Causes and lessons of five explosion accidents, J. Loss Prevent. Process Ind. 13 (2000) 439–442.
[2] CCPS, Guidelines for Chemical Process Quantitative Risk Analysis, 2nd ed., AIChE, New York, 2000, pp. 159–165.
[3] CCPS, Guidelines for Evaluating Process Plant Buildings for External Explosions and Fires, AIChE, New York, 1996, pp. 40–41.
[4] TNO Green Book, Methods for the Determination of Possible Damage, CPR 16E, TNO Green Book, Voorburg, 1989, pp. 2.11–2.12.
[5] W.E. Baker, M.J. Tang, Gas, Dust and Hybrid Explosions, Elsevier, Amsterdam, 1991, pp. 1–3.
[6] H. Phillips, Explosions in the Process Industries, 2nd ed., IChemE, Warwickshire, 1994, pp. 24–27.
[7] C.L. Mader, Numerical Modeling of Explosives and Propellants, 2nd ed., CRC Press, New York, 1996, pp. 31–32.
[8] T.C. Chapman, T.A. Rose, P.D. Smith, Blast wave simulation using AUTODYN2D: a parametric study, Int. J. Impact Eng. 16 (1995) 777–787.
[9] J.M. Powers, H. Krier, Attenuation of blast waves when detonating explosives inside barriers, J. Hazard. Mater. 13 (1986) 121–133.
[10] S. Sklavounos, F. Rigas, Validation of turbulence models in heavy gas dispersion over obstacles, J. Hazard. Mater. 108 (2004) 9–20.
[11] E. Binggeli, F. Binggeli, D. Schlapfer, K.M. Bucher, Airblast predictions in tunnel/entrance configurations due to he-detonations near the tunnel portal, in: Proceedings of the 13th International Symposium on Military Applications of Blast Simulation, Hague, The Netherlands, 1993, pp. 365–375.
[12] W.E. Baker, P.A. Cox, P.S. Westine, J.J. Kulesz, R.A. Strehlow, Explosion Hazards and Evaluation, Elsevier, Amsterdam, 1983, pp. 106–111.
[13] N.R. Popat, C.A. Catlin, B.J. Arntzen, R.P. Lindstedt, B.H. Hjertager, T. Solberg, O. Saeter, A.C. Van den Berg, Investigations to improve and assess the accuracy of computational fluid dynamic based explosion models, J. Hazard. Mater. 45 (1996) 1–25.
[14] T. Huld, G. Peter, H. Stadtke, Numerical simulation of explosion phenomena in industrial environments, J. Hazard. Mater. 46 (1996) 185–195.
[15] C.A.J. Fletcher, Computational Techniques for Fluid Dynamics, Springer-Verlag, Berlin, 1997, pp. 105–111, 400–403.
[16] T.J. Chung, Computational Fluid Dynamics, Cambridge University Press, Cambridge, 2002, pp. 262–269, 680–682, 686–692.
[17] S.H. Park, J.H. Kwon, Implementation of k-ω turbulence models in an implicit multigrid method, AIAA J. 42 (2004) 1348–1357.
[18] F.R. Menter, Two-equation eddy-viscosity turbulence models for engineering applications, AIAA J. 32 (1994) 1598–1605.
[19] H.K. Versteeg, W. Malalasekera, An Introduction to Computational Fluid Dynamics—The Finite Volume Method, Longman, New York, 1995, pp. 49–53, 114–120, 168–173.
[20] ANSYS Company, CFX-5 Solver Theory Manual CFX Ltd., ANSYS Company, Oxfordshire, 2003, pp. 57–96, 206.